Ocean-atmosphere coupled Pacific Decadal variability simulated by a climate model

Hao LUO[1,2,3], Fei ZHENG[1,4,5*], Noel KEENLYSIDE[6,7], and Jiang ZHU[8,9]

[1]*International Center for Climate and Environment Science (ICCES), Institute of Atmospheric Physics, Chinese Academy of Sciences, Beijing 100029, China*

[2]*Southern Marine Science and Engineering Guangdong Laboratory (Zhuhai), Zhuhai, China*

[3]*South China Sea Institution,and School of Atmospheric Sciences, Sun Yat-sen University, Zhuhai, China*

[4]*Collaborative Innovation Center on Forecast and Evaluation of Meteorological Disasters, Nanjing University of Information Science & Technology, Nanjing 210044, China*

[5]*Center for Ocean Mega-Science, Chinese Academy of Sciences, Qingdao 266071, China*

[6]*Geophysical Institute, University of Bergen/Bjerknes Center for Climate Research, Bergen 5007, Norway*

[7]*Nansen Environmental and Remote Sensing Center/Bjerknes Center for Climate Research, Bergen 5006, Norway*

[8]*Institute of Atmospheric Physics, Chinese Academy of Sciences, Beijing 100029, China*

[9]*University of the Chinese Academy of Sciences, Beijing 100049, China*

*Corresponding author: Dr. Fei Zheng, ICCES, Institute of Atmospheric Physics, Chinese Academy of Sciences, P.O. Box 9804, Beijing 100029, China.
Email: zhengfei@mail.iap.ac.cn

Abstract

Currently, the mechanisms for Pacific Decadal Oscillation (PDO) are still disputed, and in particular the atmosphere response to the ocean in the mid-latitude remains a key uncertainty. In this study, we investigate two potential feedbacks – a local positive and a delayed negative – for the PDO based on a long-term control simulation using the ECHAM5/MPI-OM coupled model, which is selected because of reproduces well the variability of PDO. The positive feedback is as follows. In the PDO positive phase, the meridional sea surface temperature (SST) gradient is intensified and this strengthens the lower level atmospheric baroclinicity in the mid-latitudes, leading to the enhancement of Aleutian low and zonal wind. These atmospheric changes reinforce the meridional SST temperature gradient through the divergence of ocean surface currents. The increased heat flux loss over the anomalously warm water and decreased heat flux loss over the anomalously cold water in turn reinforce the lower atmospheric meridional temperature gradient, baroclinicity and atmospheric circulation anomalies, forming a local positive feedback for the PDO. The delayed negative feedback arises, because the intensified meridional SST gradient also generates an anticyclonic wind stress in the central North Pacific, warming the upper ocean by Ekman convergence. The warm upper ocean anomalies then propagate westward and are transported to the mid-latitudes in the western North Pacific by the western boundary current. This finally reduces the meridional SST gradient, 18 years after the peak PDO phase. These results demonstrate the significant contributions of the meridional SST gradient to the PDO's evolution.

Key words: PDO, barotropic structure, feedback, meridional SST gradient, ECHAM5/MPI-OM

1. Introduction

The Pacific Decadal Oscillation (PDO) is a pattern of mid-latitude climate variability on decadal to inter-decadal time scales over the North Pacific (Mantua et al. 1997). It is commonly defined as the leading empirical orthogonal function (EOF) of North Pacific (20°–60°N) SST monthly anomalies, which are departures from the climatological annual cycle after regressing out the global mean SST changes (Newman et al. 2016). The associated principal component time series is usually regarded as the PDO index. The PDO affects the climate system in two ways. First, PDO perturbations are superimposed on long-term climate trends, thereby affecting decadal variations in climate both locally and globally. For example, PDO influences decadal climate variability over the North Pacific Ocean, North America and East China (Latif and Barnett 1994, 1996; Mantua et al. 1997; Yang et al. 2017) and likely contributed to the recent hiatus in global warming (Trenberth and Fasullo 2013). Second, the PDO provides the background state for interannual variability and may modulate it. For instance, the PDO exerts a modulating effect on ENSO (Lin et al. 2018; Vimont et al. 2001; Vimont et al. 2003) and its teleconnections (Gershunov and Barnett 1998; Wang et al. 2008; Wang and Liu 2015). Thus, the PDO has important impacts on social and economic development globally, and in particular in North America and East Asia.

Although numerous studies on the PDO and its mechanisms have been conducted since 1990, our understanding of the processes driving it remains limited, especially the existence of an atmospheric response to mid-latitude SST and its role in

71 the PDO (Newman et al. 2016). The atmospheric signature of the PDO is an
72 equivalent barotropic vertical structure, with low (high) pressure above cold (warm)
73 water (Cayan 1992a, b). The influence of the atmosphere on the mid-latitude Pacific
74 Ocean is well understood: SST is driven directly via thermodynamic interaction and
75 indirectly via changes in ocean circulation (Alexander et al. 2002; Cayan 1992a, b;
76 Latif and Keenlyside 2011; Liu and Alexander 2007). Early studies considered the
77 impact of mid-latitude ocean on the atmosphere to be weak in comparison to the
78 strong intrinsic variability of mid-latitude atmosphere (Kushnir et al. 2002).
79 Furthermore, models disagree on the atmospheric responses to mid-latitude SST
80 anomalies. Some show a barotropic response, with low pressure over cold water, or
81 with high pressure over cold water (Kushnir and Lau 1992) and others suggest a
82 baroclinic one (Hoskins and Karoly 1981). These different results from models are
83 related to differences in the atmospheric heating profiles caused by the SST anomalies
84 (Frankignoul 1985). However, recent studies based on higher resolution observations
85 and models suggest that the atmosphere does respond to the SST anomalies in western
86 boundary current regions, particularly the subarctic frontal zone (Ma et al. 2015; Ma
87 et al. 2016; Nakamura et al. 2004; O'Reilly and Czaja 2015; Small et al. 2008). In this
88 region, persistent SST anomalies in winter tend to change the state of atmosphere
89 through heat and moisture fluxes (Taguchi et al. 2012), and these atmosphere
90 anomalies in turn affect the ocean state (Qiu and Chen 2005; Qiu et al. 2007).
91 Although possibly weaker than observed, these feedbacks might be active also in
92 lower resolution climate models (Latif 2006; Latif and Barnett 1994, 1996; Park and

93 Latif 2010; Zhang and Delworth 2015). Thus, this atmospheric response to
94 mid-latitude SST anomalies can be important in decadal climate variability (Fang and
95 Yang 2016; Kwon and Deser 2007; Zhong et al. 2008; Zhou et al. 2015), and
96 understanding it is critical for the simulation and prediction of PDO.

97 The mechanisms raised to driving the PDO in previous studies could be broadly
98 divided into three categories. First, the PDO is driven by the stochastic forcing of the
99 atmosphere. From this perspective, high frequency weather fluctuations excite low
100 frequency ocean variations (e.g., Frankignoul et al. 1997; Jin 1997; Latif and
101 Keenlyside 2011). While the stochastic forcing does not depend on an atmospheric
102 response to the developing ocean anomalies, it can be important in sustaining a
103 damped coupled mode (Latif and Keenlyside 2011). Furthermore, an atmospheric
104 response to mid-latitude SST anomalies could enhance the decadal variance, or lead
105 to a preferred time scale, if the response is a positive or delayed negative, respectively,
106 feedback on the low-frequency variability (Barsugli and Battisti 1998; Frankignoul
107 1985; Lee et al. 2008; Sura et al. 2006). Second, the PDO is driven by teleconnection
108 from the tropics (Newman et al. 2003; Shakun and Shaman 2009). In this case,
109 tropical variability, such as ENSO or the decadal variability of ENSO, drives
110 variability in the North Pacific by the atmosphere (e.g., Alexander et al. 2002;
111 Trenberth et al. 1998) and/or ocean (e.g., Gu and Philander 1997; Kleeman et al.
112 1999). Besides, two-way interactions between the tropical and North Pacific may
113 impact low-frequency variability in both domains (e.g., Newman 2007; Solomon et al.
114 2003). Third, the PDO is driven by mid-latitude air–sea interactions. In this viewpoint,

115 the unstable ocean–atmosphere interactions in the mid-latitude would lead to the PDO
116 (Fang and Yang 2011, 2016; Latif and Barnett 1994, 1996; Zhang and Delworth 2015).
117 Besides, compared to the limited predictive skill resulting from stochastic forcing,
118 predictability may be potentially enhanced by taking into account the air-sea
119 interaction (Barnett et al. 1999; Pierce 2001). Thus, the PDO can be regarded as a
120 result of a combination of different physical processes, but the relative importance of
121 these, especially the third, remains uncertain (Newman et al. 2016). In this study, a
122 coupled general circulation model (CGCM) developed at the Max Planck Institute
123 that reproduces well the key features of the PDO is used to investigate the structure
124 and possible feedback mechanisms of the PDO.

125 The remainder of the paper is organized as follows. The model and data used are
126 described in Section 2. In Section 3, the typical structure of the wintertime PDO in
127 CGCM is presented. Feedbacks in CGCM to maintain or reverse the phase of the
128 PDO are examined in Sections 4.1 and 4.2, respectively. The final section is the
129 conclusions and discussion.

130

131 2. Methodology

132 *2.1. Model*

133 The current analysis employs a coupled atmosphere-ocean general circulation
134 model of the Max Planck Institute (ECHAM5/MPI-OM) (Jungclaus et al. 2006) to
135 explore the possible mechanism for the PDO. The fifth-generation atmospheric
136 general circulation model (ECHAM5) has been developed from the European Center

for Medium range Weather Forecasting operational forecast model cycle 36 (1989) and a comprehensive parameterization package developed at Hamburg. It is run at T63 resolution (1.875°× 1.875°) with 31 vertical (hybrid) levels. The Max–Planck–Institute ocean model (MPI-OM) has been derived from the Hamburg Ocean Primitive Equation model, which simulates the primitive equations for a hydrostatic Boussinesq fluid with a free surface and includes an embedded sea ice model. It has 1.5° average horizontal grid spacing with 40 unevenly spaced vertical levels from 6 m to 5720 m. More technical details of ECHAM5 and MPI-OM can be found in Roeckner et al. (2003) and Marsland et al. (2003). The atmosphere and ocean are coupled once a day via the Ocean–Atmosphere–Sea Ice–Soil (OASIS) coupler (Valcke et al. 2003). The ocean passes SST, sea ice concentration, sea ice thickness, snow depth, and ocean surface velocities to the atmosphere, whereas the atmosphere passes surface wind stress, fresh water flux, and heat flux to the ocean. No flux adjustment is applied. This study use monthly data from a pre-industrial control experiment of ECHAM5/MPI-OM that excludes the effect of human activities by imposing non-evolving pre-industrial conditions. Thus, here we consider the PDO as a natural pattern of climate variability resulting from dynamics internal to the climate system. In this study, we conduct a 600–year control simulation (Zheng 2014), and analyze the last 150 years of the result; the PDO in this period shows very similar characteristics to the PDO of the entire run.

2.2. Data

We use monthly mean observations from 1854 to 2014, including sea surface temperature (SST) and atmospheric circulation data, to evaluate the performance of ECHAM5/MPI-OM. The SST data are the Extended Reconstructed Sea Surface Temperature version 3b (ERSST V3b) (Smith et al. 2008): a global SST analysis with a 2° horizontal resolution and derived from the International Comprehensive Ocean–Atmosphere Dataset with missing data filled in by statistical methods. The atmospheric circulation data are the Twentieth Century Atmospheric Reanalysis version 2c (20CRv2c) (Compo et al. 2011), which assimilates only surface pressure reports and uses observed monthly sea-surface temperature and sea-ice distributions as boundary conditions. It provides an estimate of the global tropospheric variability with a 2° spatial resolution.

In this study, winter (DJF) refers to the months of December, January, and February. Interannual anomalies are obtained by removing the mean seasonal cycle from the original fields. Furthermore, the atmospheric baroclinicity is represented by the Eady growth rate, which is calculated according to the relation

$$\sigma_{BI} = \frac{0.31 f \frac{\partial u}{\partial z}}{N}$$

$$N^2 = \frac{g}{\bar{\theta}} \frac{d\bar{\theta}}{dz}$$

where f is the Coriolis parameter, u is the zonal wind, N^2 is the buoyancy frequency or the Brunt–Vaisala frequency, g is the gravitational acceleration, and $\bar{\theta}$ is the potential temperature of the background state.

3. Structure of the PDO

ECHAM5/MPI-OM realistically simulates the PDO SST structure and timescale. As in the observations, the model simulated PDO shows SST variations with negative anomalies over the central and western mid-latitude North Pacific, surrounded by positive anomalies (Fig. 1a,b). Besides, the maximum zone of negative climatological meridional SST gradient nearly overlays in the western cooling region during the PDO positive phase, implying the SST gradient increasing south of cooling center while decreasing north of that. In the model, however, the negative anomalies are located further to the west compared to observations and the positive anomalies further to the North. Furthermore, the coupled model captures the main periodicities of the observed PDO (Figs. 1c-f).

The atmospheric and oceanic structure of the PDO in DJF is investigated by composite analysis in both observations and simulations, considering the difference between periods when the index is above and below one standard deviation. During the positive PDO phase, SST is anomalously cold in the western-to-central North Pacific but warm off the west coast of North America and in low latitudes (Fig. 2). This pattern leads to an southward shift of the SST gradient in the western Pacific around 40°N. The SLP becomes low over the North Pacific, reflecting an enhanced Aleutian low. Over the cooling SST center, the air temperature is anomalously cold in lower layers of the troposphere but warm in upper layers. In contrast to the variation of air temperature, the geopotential height decreases in the whole troposphere. This observed relationship between the atmosphere and the ocean also exists in our

simulations, although the simulated structure locates further west compared to the observation. In summary, north-east of the cold SST anomaly, the geopotential height anomaly displays an equivalent barotropic low from the surface to 100 hPa. This kind of vertical structure is dubbed an equivalent barotropic cold/trough structure, and characterizes the configuration of the mid-latitude North Pacific ocean–atmosphere anomalies on the decadal time scale.

It should be noticed that the above-mentioned vertical structure differs from that in the tropics that is primarily thermal-driven (Gill 1980; Matsuno 1966). In the thermal-driven situation, when the underlying temperature becomes cold, a baroclinic response in the pressure field occurs, with increases in geopotential height at lower layers and decreases in upper layers. Therefore, the feedback in the mid-latitude North Pacific should also be considered differently from that in the tropics (Hoskins and Karoly 1981). In the following sections, we focus on a positive feedback that enhances this structure, and a delayed negative feedback that causes the transition between phases.

4. Mechanism for the PDO in ECHAM5/MPI-OM

4.1. Positive feedback of the PDO

Given the typical time scale of the mid-latitude upper ocean, the mid-latitude ocean–atmosphere interaction is often considered as a potential source of decadal-to-interdecadal climate variability (Mantua et al. 1997; Trenberth 1990). Therefore, we focus on the region within 20°N–60°N, and 150°E –150°W to

224 investigate the local ocean–atmosphere feedback, through linear regression of DJF
225 anomalies on the wintertime PDO index. This region is indicated in Fig. 2 by a yellow
226 box.

227 Climatologically, the relationship between the atmospheric transient eddy
228 activities and the mean flow were previously identified with zonal averages over
229 whole Northern Hemisphere (Holopainen et al. 1982; Lau and Holopainen 1984).
230 Meanwhile, the transient eddy activities build a bridge of the atmospheric response to
231 midlatitude SST anomalies. Thus, we use zonal averages over the midlatitude North
232 Pacific (the yellow one in Fig. 2) to identify the atmospheric response to midlatitude
233 SST anomalies. The zonal average meridional gradient of SST is negative in this
234 region. Two maximum values exist at around 26°N and 42°N that correspond to the
235 subtropical and subarctic oceanic frontal zones, respectively (Fig. 3a). The subtropical
236 oceanic frontal zone is associated with wind–driven submesoscale subduction
237 (Hosegood et al. 2013), whereas the subarctic zone is caused by the confluence of
238 warm Kuroshio and cold Oyashio (Talley et al. 2011). During the PDO positive phase,
239 the tripole SST anomalies with cooling in the mid-latitude western North Pacific and
240 warming to the north and south of it (Fig. 2) causes the meridional gradient of SST to
241 intensify to the south of 40°N and weaken north of it (Fig. 3a), implying that the
242 subarctic oceanic front zone moves southward. As the language of ocean–atmosphere
243 communication, the surface heat flux plays an important role in the information
244 transfer between the ocean and atmosphere. And differential air-sea heat exchanges
245 across an oceanic frontal zone maintain lower level atmospheric baroclinicity (e.g.,

Kuwano-Yoshida and Minobe 2017; Nakamura et al. 2004; Taguchi et al. 2012). The ocean is cooler than the atmosphere, and obtains fresh water in the north of 40°N; while the ocean is warmer than the atmosphere, and loses fresh water in the south. Thus, the sensible heat flux as well as the latent heat flux would be transferred to the ocean in the north of 40°N while to the atmosphere in the south of 40°N. The anomalous net surface heat flux acts as a diabatic heating source of the lower troposphere to the south of 40°N and a heating sink to the north, and these are determined by the latent and sensible heat flux. It is worth noting that these characters in Fig. 3a are consistent to those in the KOE region, as the air-sea flux are strongest in the KOE region (Kelly et al. 2010; Kwon et al. 2010; Qiu et al. 2007; Taguchi et al. 2012). Thereby the ocean enhances the meridional air temperature gradient in low levels, with a maximum at 600 hPa (Fig. 3b). According to the thermal wind equation, the vertical shear of zonal wind is proportional to the meridional gradient of temperature. Therefore, the change in the Eady growth rate (Fig. 3c) is similar to that of the meridional gradient of temperature, indicating that the ocean maintains the anomalous mid-to-low tropospheric baroclinicity (Fig. 3c). This favours an increase in atmospheric transient eddies, and in the poleward flux of heat and momentum in the atmosphere, that alters the large-scale atmospheric circulation (Brayshaw et al. 2008; Holton 2004; Hoskins and Valdes 1990; Nakamura et al. 2008). Besides these, previous studies highlight the importance of diabatic heating on this issue: The latent heating anomalies to the south likely explain the mid-tropospheric heating that has been linked to synoptic scale variations (Papritz and Spengler 2015). And there is

evidence that such diabatic heating associated with anomalies in SST fronts influences extreme synoptic scale variability and in turn the Aleutian low in late winter (Kuwano-Yoshida and Minobe 2017).

Thus, the influence of mid-latitude ocean anomaly on the atmosphere may be through not only diabatic heating but also the transient eddies. To assess these processes quantitatively, an analysis based on the quasi-geostrophic potential vorticity (QGPV) equation is performed. The QGPV equation (Fang and Yang 2016; Taguchi et al. 2012) is described as follows:

$$\left(\frac{\partial}{\partial t}+\bar{\vec{V}}_h\cdot\nabla\right)\left[\frac{1}{f}\nabla^2\bar{\phi}+f+\frac{\partial}{\partial p}\left(\frac{f}{\sigma_1}\frac{\partial\bar{\phi}}{\partial p}\right)\right]=-f\frac{\partial}{\partial p}\left(\frac{\alpha}{\sigma_1}\frac{\bar{Q}_d}{\bar{T}}\right)-f\frac{\partial}{\partial p}\left(\frac{\alpha}{\sigma_1}\frac{\bar{Q}_{eddy}}{\bar{T}}\right)+\bar{F}_{eddy},$$

where overbars indicates the seasonal mean. The variables ϕ, $\vec{V}_h$, f, α σ_1 and T indicate the geopotential height, the geostrophic wind, the Coriolis parameter, the Specific volume, the static stability parameter and the temperature, respectively. $\bar{Q}_d$ is the seasonal-mean diabatic heating derived from the residual of the thermodynamic equation (Yanai and Tomita 1998). $\bar{Q}_{eddy}$ is the seasonal-mean transient eddy heating expressed as,

$$Q_{eddy}=-\nabla\cdot\overline{\vec{V}_h'T'}-\frac{\partial\overline{\omega'T'}}{\partial \mathrm{p}}+\frac{R}{C_pP}\overline{\omega'T'},$$

where the prime indicates the departure from the seasonal mean. The variables ω, R and C_p indicate the vertical velocity, the gas constant for dry air and the specific heat of dry air at constant pressure. $\bar{F}_{eddy}$ is the transient eddy vorticity forcing written as,

$$\bar{F}_{eddy}=-\nabla\cdot\overline{\vec{V}_h'\zeta'},$$

where variable ζ indicates the vorticity.

As Figure 4 shows, the diabatic heating is centered below the middle troposphere, with a maximum at 850 hPa (Fig. 4a), unlike that induced by convection in the tropics. According to the QGPV equation, this shallow diabatic heating tends to decrease the geopotential height below 850hPa and increase above. Thus, the Aleutian low is deepened near the surface via the diabatic heating. And the thermal transport by the transient eddy activities converges north of 40°N with a maximum at 300 hPa (Fig. 4b). This transient eddy heating centered at the mid-troposphere can also reduce the geopotential height in a similar manner as the diabatic heating. Thus, both diabatic heating and transient eddy heating create a baroclinic atmospheric response, which suggest to deepen the Aleutian low in the lower-to-middle troposphere. Furthermore, transient eddies also transport vorticity flux in the upper troposphere. The convergence of vorticity flux by transient eddy activities produces a maximum at 300hPa (Fig. 4c), which generates a barotropic response and reduces the geopotential height in the upper troposphere. Consequently, as a joint result of thermal and eddy driving, the Aleutian low is enhanced in the whole troposphere (Fig. 4d).

Accompanied with the deepened Aleutian low, the surface zonal wind is enhanced as shown in Fig. 5a, especially the westerly wind to the north of negative SST anomalies, resulting in changes in ocean circulation. To investigate the influence of ocean circulation changes in SST, the SST tendency induced by advections, namely $-\left(\vec{V}\cdot\nabla T\right)' = -\left(u\frac{\partial T}{\partial x} + v\frac{\partial T}{\partial y} + w\frac{\partial T}{\partial z}\right)'$, is displayed in Fig. 5b. The anomalous advection of SST can cause a large-scale SST cooling in the North Pacific, which

covers the cooling center during the PDO positive phase. Therefore, through the ocean dynamical processes forced by the increased surface westerly, the original cold SST anomaly will be sustained or even intensified, leading to the maintenance or enhancement of the SST gradient anomaly, which is important to balance the damping effect of atmosphere on the ocean via the surface heat flux (Fig. 3a).

Figure 6 provides a schematic summary of the local positive feedback. During the positive phase, the cooling of SST at the North Pacific enhances the meridional gradient of SST south of 40°N. The corresponding increased heat to the south and cooling to the north of the climatological SST front, acts to enhance the gradient of atmospheric temperature and the atmospheric baroclinicity, which favour increased atmospheric transient eddy activity. The increased transient eddy activity and diabatic heating deepen the Aleutian low and drive stronger westerlies. These phenomena result in a large-scale SST cooling in the North Pacific through the ocean dynamical processes. Consequently, this maintains or even enhances the meridional SST gradient anomalies.

4.2. Delayed negative feedback in the PDO

The previous section describes the positive feedbacks amplifying PDO anomalies, but a negative feedback is required to transform the PDO to the opposite phase. The PDO pattern shows opposite SST anomalies in the lower latitudes of the Pacific compared to those in the western-to-central North Pacific (Fig. 2). Hence, we focus on the air-sea interaction and upper ocean processes related to the transport of

334 warm water and formation of upper ocean heat content anomalies in the mid-latitude
335 on decadal time scales. All variables are subjected to a 10-yr low-pass Lanczos filter
336 to obtain their decadal components in this section.

337 Figure 7 presents the correlation between the PDO index and the wind stress curl
338 anomalies. At the peak phase of the PDO, the wind stress curl (Fig. 7) shows a dipole
339 pattern in the meridional direction in the central Pacific, with positive values in the
340 subpolar region and negative values in the subtropics. These are consistent with the
341 enhanced surface westerlies during when the PDO is at peak phase (Fig. 5a).
342 Although the significant wind stress curl anomaly appears over the subpolar ocean in
343 ECHAM5/MPI-OM, it does not produce the significantly opposite upper ocean
344 temperature anomaly in the subpolar subsurface, compared to the anomaly in the
345 Kuroshio–Oyashio Extension (KOE) region, which thus does not contribute to a
346 delayed negative feedback. While according to Qiu et al. (2007), the wind stress curl
347 anomaly in the subtropical plays an important role in the phase reversal of the PDO.
348 Thus, a wind stress curl index is defined as the negative of surface wind stress curl
349 anomalies averaged for the area 170°E - 150°W and 20°N - 36°N, which is indicated
350 in Fig. 7a by a green box. To further investigate the evolution of the PDO, we adopt
351 lagged correlation analysis hereafter. The lagged correlation between the PDO index
352 and related variables is described as follows:

353 $$r(m) = \frac{\langle PDO(t)var(t+m)\rangle}{\sqrt{\langle PDO^2(t)\rangle\langle var^2(t+m)\rangle}}$$

354 where PDO and var indicate the PDO index and related variables, respectively.
355 Angle brackets denote the time average and m (>0) denotes the PDO index lead time

356 in years. For example, if $m = 1$ (i.e., the x-coordinate is 1 in Fig. 7b), it means the
357 PDO index leads related variables by one year. Fig. 7b shows that there is a persistent
358 influence of ocean on atmosphere from -1 to +3 years lag, as the correlation between
359 the low-frequency filtered wind stress curl and PDO indices reaches the peak when
360 the wind stress curl index lags the PDO by approximately 1 year.

361 Decadal variability of SST mainly originates from the long-term memory of
362 ocean, particularly from the subsurface process. Thus, analysis of the upper ocean
363 heat content, which includes ocean subsurface signals, is appropriate to understand
364 the mechanisms contributing to decadal variability. To investigate the impact of
365 surface wind stress on the upper ocean, the lagged correlation between the upper
366 700m ocean heat content (OHC700) and the wind stress curl index are displayed in
367 Figure 8. The OHC700 is selected to represent the state of upper ocean, considering
368 the dynamical ocean response to wind forcing as well as the thermocline depth of
369 North Pacific. As Fig. 8a shows, the negative wind stress curl anomalies increase the
370 upper ocean heat content through Ekman convergence in the low latitudes of central
371 Pacific; they exert a continuous influence on the upper ocean caused by persistent
372 anticyclonic wind stress anomalies (Fig. 7). These positive OHC700 anomalies move
373 westward from the ocean interior into the western boundary current (WBC) region
374 (Fig. 8b). When these positive anomalies reach the west Pacific, they warm the WBC
375 region, and are transported by the Kuroshio (Fig 8c). Finally, these positive OHC700
376 anomalies move northward and warm the western-to-central North Pacific (Fig. 8d),
377 and this results in the transition of PDO from positive phase to negative phase after

about 18 years. In addition, there is no obvious warm advection of ocean heat content from the subpolar to the KOE region along the Oyashio throughout the entire evolution.

To further clarify the role of oceanic Rossby wave in the evolution of the PDO, the sea surface height (SSH) is used to represent the variation of upper ocean. The evolution of SSH anomalies associated with the PDO is shown as the lagged correlation of SSH upon the PDO index (Fig. 9). The positive SSH anomalies appears in the central Pacific at a lag of 0 yr, caused by the anticyclonic wind stress anomalies in the subtropical (Fig. 7). As we move forward from lag 0, the positive SSH anomaly gradually propagates westward, and finally reaches the WBC region at a lag of around 5 yr. Subsequently, the negative SSH anomaly appears in the central Pacific. Therefore, considering the phase speed of oceanic Rossby wave in the midlatitude as well as the position of wind stress curl anomaly (Zhang and Delworth 2015, 2016), this phenomenon indicates westward propagation of the OHC700 is caused by free Rossby waves in the subtropical ocean interior.

Considering the dominant role of the WBC in the heat transported poleward by the oceans (Kelly and Dong 2004), the lag correlation between PDO index and each term of local heat budget over the upper 700 m is performed to isolate the advection through the Kuroshio in WBC regions (Fig. 10). The local heat budget is described in the following equation:

398 $$\frac{\partial T'}{\partial \mathrm{t}} = -\left(\overline{u}\frac{\partial T'}{\partial x} + u'\frac{\partial \overline{T}}{\partial x} + u'\frac{\partial T'}{\partial x}\right) - \left(\overline{v}\frac{\partial T'}{\partial y} + v'\frac{\partial \overline{T}}{\partial y} + v'\frac{\partial T'}{\partial y}\right)$$

399 $$-\left(\overline{w}\frac{\partial T'}{\partial z} + w'\frac{\partial \overline{T}}{\partial z} + w'\frac{\partial T'}{\partial z}\right) + \frac{Q'}{\rho C_p H} + R$$

400 where overbars and primes indicate the monthly climatology and anomaly,
401 respectively. The variables u, v, w, and T indicate zonal current, meridional current,
402 vertical velocity, and oceanic temperature averaged over the upper 700 m, respectively.
403 Q is the net surface heat flux into the ocean, ρ is the density of seawater, C_p is the
404 heat capacity of sea water, and R is the residual term. The first four groups of terms on
405 the right-hand side of the equation represent advection in the zonal, meridional,
406 vertical directions, and heat flux, respectively.

407 As Fig. 10a shows, the decadal SST tendency is mainly associated with the
408 meridional temperature advection over the Kuroshio region (indicated by the yellow
409 box in Fig. 8), while heat flux and zonal and vertical temperature advection act as
410 damping terms. A decomposition of the meridional temperature advection term finds
411 that the term related to the mean current and the anomalous temperature gradient
412 ($-\overline{v}\frac{\partial T'}{\partial y}$) is dominant. While over the KOE region (indicated by the green box in Fig.
413 8), the decadal SST tendency is in phase with the zonal temperature advection,
414 whereas heat flux and zonal and vertical temperature advection are out of phase
415 (Fig.10b). A decomposition of the zonal temperature advection term finds that the
416 term related to the mean current and the anomalous temperature gradient ($-\overline{u}\frac{\partial T'}{\partial x}$) is
417 dominant. These results suggest the essential role of climatological current field on
418 the evolution of upper ocean in the WBC regions. The significant warm anomalies

419 appear in the Kuroshio region at a lag of 5 yr, when the downwelling Rossby wave
420 reaches this region, and they reach their peak at a lag of 10 yr. In addition, it is worth
421 noting that there are significant warm anomalies in the KOE region at a lag of 16 yr,
422 and warm anomalies reach the peak at a lag of 18 yr; these are consistent with Figs.
423 8b-c. The above results demonstrate that it takes 18 years to complete the transition
424 from cool phase to warm phase in the KOE region; this is approximately equal to half
425 the PDO period (i.e., about 37 years).

426 To further validate the oscillation on decadal timescales, multichannel singular
427 spectrum analysis (M-SSA) is applied in this study, which is a natural extension of
428 SSA to multiple short noisy time series (Ghil et al. 2002). SSA is mathematically
429 equivalent to the extended EOF analysis, and both are extensions of classical principal
430 component analysis. However, the two methods differ in emphasis: extended EOF
431 analysis usually chooses a number of spatial channels much greater than the number
432 of temporal lags, thus limiting the temporal and spectral information. In MSSA, the
433 situation is the reverse, where the number of temporal lags is large enough to extract
434 detailed temporal and spectral information from the multivariate time series. The
435 advantage over classical spectral analysis is that SSA/M-SSA allows anharmonic
436 behavior to be depicted by a pair of eigenvectors and temporal variations of the
437 amplitude of the oscillatory behavior to be captured.

438 Here, M-SSA is applied to first ten leading PCA components of SST, OHC700
439 and wind stress curl over the North Pacific, and three oscillatory modes can be found
440 on decadal timescales, whose period represents 37, 20 as well as 14 years,

441 respectively. Then, according to Plaut and Vautard (1994), the space-time behavior of
442 the decadal oscillation is investigated by performing a composite analysis keyed to the
443 phases of the oscillation (Fig. 11). In phase 1, negative OHC700 appear over the
444 central and western mid-latitude North Pacific, surrounded by positive anomalies,
445 which indicates the positive phase of PDO. Meanwhile, the anticyclonic wind stress
446 arises over the subtropics and is sustained to phase 2. Through the influence of
447 above-mentioned wind stress, the positive OHC700 arises in the subtropics,
448 propagates westward, and gradually reverses the PDO phase in the following phases,
449 consistent with results of lag correlation. It is worth noting that the cyclonic wind
450 stress is organized at the negative phase of PDO (phase 4). In addition, the evolution
451 of SST is similar that of OHC700, implying the importance of subsurface ocean
452 temperature on the PDO. The OHC700 anomalies over the subpolar gyre region do
453 not seem to be consistent with the wind stress curl, rather these anomalies are
454 consistent with heat flux (Fig. 3a). The wind stress curl anomalies in the subpolar gyre
455 region are also not reversed in phase 4, suggesting that in this region they do not play
456 an important role for the PDO reversal.

457 According to the above-mentioned processes, a decadal time scale, delayed
458 negative feedback for the PDO emerges (Fig. 12). During the positive phase, the
459 cooling of SST at the North Pacific enhances the meridional gradient of SST south of
460 40°N. Therefore, the westerly wind is enhanced and the anticyclonic wind stress
461 anomalies are produced on the south side of westerlies. Consequently, these
462 anticyclonic wind stress anomalies excite the positive OHC700 anomalies by Ekman

463 convergence, and positive OHC700 anomalies propagate westward as the oceanic
464 Rossby wave. When positive OHC700 anomalies reach the western boundary, they
465 warm the WBC region and are transported through the Kuroshio. This eventually
466 leads to warm SST anomalies in the western-to-central North Pacific and reduces the
467 meridional SST gradient south of 40°N, thereby switching the phase of PDO
468 gradually.
469

470 5. Conclusions and discussion

471 The PDO is characterized by a horseshoe pattern of SST anomalies with one sign
472 in the western-to-central North Pacific surrounded by anomalies of opposite sign. It is
473 an important climate variation on decadal timescales that has a major influence on
474 climate system. Understanding the mechanism of the PDO is therefore of broad
475 scientific and socioeconomic interest, but understanding remains limited, especially of
476 the role of extra-tropical ocean–atmosphere interaction in the PDO. This paper
477 reinvestigates the mechanisms for the PDO focusing on this last aspect and using a
478 150-year preindustrial control simulation of ECHAM5/MPI-OM, which reproduces
479 key features of the PDO very well. The simulated positive (negative) PDO exhibits a
480 large-scale SST cooling (warming) over the central and western mid-latitude North
481 Pacific, and the atmospheric geopotential height shows an equivalent barotropic low
482 (high) anomaly throughout the troposphere associated with the enhanced (weakened)
483 zonal wind. This equivalent barotropic cold/trough structure is the typical structure of
484 the observed PDO during winter. Based on the meridional SST gradient in the KOE

485 region, we identify two possible feedbacks – a positive and a delayed negative – that
486 may sustain the PDO.

487 The positive feedback process to maintain the structure of PDO is as follows.
488 During the positive (negative) PDO phase, the cooling (warming) of SST at the North
489 Pacific enhances (reduces) the meridional SST gradient south of 40°N. The
490 subsequent change in net surface heat flux damps the meridional gradient of SST, and
491 provides the diabatic heat driving the increased (decreased) meridional gradient of
492 atmosphere temperature as well as baroclinicity in mid-to-lower levels. This favours
493 (suppresses) transient atmospheric variability and diabatic heating. The atmospheric
494 response to either shallow diabatic heating (cooling) or deep transient eddy heating
495 (cooling) is dynamically baroclinic, whereas the response to the transient eddy
496 vorticity forcing is equivalent barotropic. These intensify (weaken) the Aleutian low.
497 The stronger westerlies result in the ocean dynamical processes, which is important to
498 balance the damping effect of surface heat flux on the ocean. Consequently, they will
499 reinforce the enhanced meridional SST gradient south of 40°N.

500 The delayed negative feedback reversing the PDO phase on decadal timescales is
501 summarized as follows. During the positive (negative) phase, the SST is cold (warm)
502 in the North Pacific and the meridional SST gradient is intensified (weakened) south
503 of 40°N. Therefore, the westerly wind is intensified (reduced) and the anticyclonic
504 (cyclonic) wind stress anomalies are produced on the south side of westerlies. Then,
505 these anticyclonic (cyclonic) wind stress anomalies excite the warm (cold) upper
506 ocean anomalies by Ekman convergence (divergence). These upper ocean anomalies

propagate westward from the ocean interior into the WBC region, with a speed consistent of free Rossby waves. When they reach the western boundary, they are transported by the Kuroshio as well as the KOE, and reverse the sign of the preexisting PDO and the meridional SST gradient gradually.

Our conclusion that mid-latitude ocean-atmosphere interaction can play an important role in the evolution of PDO is consistent with other studies (e.g., Latif 2006; Latif and Barnett 1994, 1996; Park and Latif 2010; Zhang and Delworth 2015). However in contrast to these, our work clearly shows that the meridional SST gradient in the KOE region plays an essential role in the positive and the delayed negative feedbacks, due to its influence on the internal atmospheric variability through not only direct diabatic heating but indirect transient eddy forcing. Although the feedback proposed in this study is based on the results from ECHAM5/MPI-OM, the types of feedback coincide with those in observations (Fang and Yang 2016; Latif and Barnett 1996; Qiu et al. 2007). The positive and negative feedback constitute a complete evolution of the atmosphere and ocean that is useful for understanding the oscillatory mechanism of the PDO. The results here are obtained from only one single model, and the robustness of feedbacks identified here should be confirmed in other models. In particular, it is important to understand whether the strength of the feedbacks is realistically reproduced. This question is difficult to address and beyond the scope of this work. However, there is some evidence from models with higher resolution than used here (e.g., Ma et al. 2015; Ma et al. 2016; O'Reilly and Czaja 2015; Zhou et al. 2015) and climate predictions (Scaife and Smith 2018) that the strength of

mid-latitude ocean-atmosphere interaction in current climate models is underestimated.

In addition, some other important mechanisms on modulating PDO, such as the atmospheric bridge (Alexander et al. 2002; Trenberth et al. 1998) and the extratropical–tropical interaction (Gu and Philander 1997; McPhaden and Zhang 2002), are not discussed in this paper. In the present study, we only focused on the influence of mid-latitude air-sea interaction on the PDO. Therefore, assessing the relative importance of various mechanisms would be an important aspect in future works. Besides, climate variability is influenced by initial conditions as well as external forcing (e.g., Meehl et al. 2014), and data assimilation can provide better constraints on initial conditions for climate simulations and predictions (e.g., Keenlyside et al. 2005; Keenlyside et al. 2008; Zheng and Zhu 2010; Zheng et al. 2007; Zheng et al. 2006). Thus, in a following work we will conduct a quantitative study via the established data assimilation system (Luo et al. 2017) to confirm the relevance of the mechanism of this study. For example, we can reproduce the meridional SST gradient in the KOE region, by assimilating SST, to investigate to what extent the atmospheric anomalies are reproduced under this SST gradient structure. And we can reconstruct the variability of tropical Pacific, through only assimilating SST in the tropical Pacific, to quantify the contribution of tropical Pacific on the PDO and to explore underlying mechanisms.

Acknowledgments

This work was supported by the National Key R&D Program of China (Grant No. 2017YFA0604201), the National Natural Science Foundation of China (Grant Nos. 41876012; 41861144015), and the program of CAS (Grant No. ZDBS-LY-DQC010). Noel Keenlyside was supported by the ERC (Grant No. 648982). The ERSST V3b data are available from https://www.esrl.noaa.gov/psd/data/gridded/data.noaa.ersst.v3.html. The 20CRv2c data are available from https://www.esrl.noaa.gov/psd/data/gridded/data.20thC_ReanV2c.html.

References

Alexander MA, Blade I, Newman M, Lanzante JR, Lau N-C, Scott JD (2002) The atmospheric bridge: The influence of ENSO teleconnections on air-sea interaction over the global oceans. J Clim 15:2205-2231. https://doi.org/10.1175/1520-0442(2002)015<2205:tabtio>2.0.co;2

Barnett TP, Pierce DW, Saravanan R, Schneider N, Dommenget D, Latif M (1999) Origins of the midlatitude Pacific decadal variability. Geophys Res Lett 26:1453-1456. https://doi.org/doi:10.1029/1999GL900278

Barsugli JJ, Battisti DS (1998) The basic effects of atmosphere–ocean thermal coupling on midlatitude variability. J Atmos Sci 55:477-493. https://doi.org/10.1175/1520-0469(1998)055<0477:Tbeoao>2.0.Co;2

Brayshaw DJ, Hoskins BJ, Blackburn M (2008) The storm-track response to idealized SST perturbations in an aquaplanet GCM. J Atmos Sci 65:2842-2860. https://doi.org/10.1175/2008jas2657.1

Cayan DR (1992a) Latent and sensible heat flux anomalies over the northern oceans: Driving the sea-surface temperature. J Phys Oceanogr 22:859-881. https://doi.org/10.1175/1520-0485(1992)022<0859:lashfa>2.0.co;2

Cayan DR (1992b) Latent and sensible heat flux anomalies over the northern oceans: The connection to monthly atmospheric circulation. J Clim 5:354-369. https://doi.org/10.1175/1520-0442(1992)005<0354:lashfa>2.0.co;2

Compo GP et al. (2011) The twentieth century reanalysis project. Q J R Meteorol Soc 137:1-28. https://doi.org/10.1002/qj.776

581 Fang J-B, Yang X-Q (2011) The relative roles of different physical processes in the
582 unstable midlatitude ocean–atmosphere interactions. J Clim 24:1542-1558.
583 https://doi.org/10.1175/2010jcli3618.1
584 Fang J-B, Yang X-Q (2016) Structure and dynamics of decadal anomalies in the
585 wintertime midlatitude North Pacific ocean-atmosphere system. Clim Dyn
586 47:1989-2007. https://doi.org/10.1007/s00382-015-2946-x
587 Frankignoul C (1985) Sea surface temperature anomalies, planetary waves, and
588 air-sea feedback in the middle latitudes. Rev Geophys 23:357-390.
589 https://doi.org/10.1029/RG023i004p00357
590 Frankignoul C, Muller P, Zorita E (1997) A simple model of the decadal response of
591 the ocean to stochastic wind forcing. J Phys Oceanogr 27:1533-1546.
592 https://doi.org/10.1175/1520-0485(1997)027<1533:asmotd>2.0.co;2
593 Gershunov A, Barnett TP (1998) Interdecadal modulation of ENSO teleconnections.
594 Bull Am Meteorol Soc 79:2715-2725.
595 https://doi.org/10.1175/1520-0477(1998)079<2715:imoet>2.0.co;2
596 Ghil M et al. (2002) Advanced spectral methods for climatic time series. Rev
597 Geophys 40:1003. https://doi.org/10.1029/2000rg000092
598 Gill AE (1980) Some simple solutions for heat-induced tropical circulation. Q J R
599 Meteorol Soc 106:447-462. https://doi.org/10.1256/smsqj.44904
600 Gu D-F, Philander SGH (1997) Interdecadal climate fluctuations that depend on
601 exchanges between the tropics and extratropics. Science 275:805-807.
602 https://doi.org/10.1126/science.275.5301.805

603 Holopainen EO, Rontu L, Lau N-C (1982) The effect of large-scale transient eddies
604 on the time-mean flow in the atmosphere. J Atmos Sci 39:1972-1984.
605 https://doi.org/10.1175/1520-0469(1982)039<1972:Teolst>2.0.Co;2
606 Holton JR (2004) An introduction to dynamic meteorology. 4th edn. Academic Press,
607 San Diego, CA
608 Hosegood PJ, Gregg MC, Alford MH (2013) Wind-driven submesoscale subduction at
609 the North Pacific subtropical front. J Geophys Res Oceans 118:5333-5352.
610 https://doi.org/10.1002/jgrc.20385
611 Hoskins BJ, Karoly DJ (1981) The steady linear response of a spherical atmosphere to
612 thermal and orographic forcing. J Atmos Sci 38:1179-1196.
613 https://doi.org/10.1175/1520-0469(1981)038<1179:tslroa>2.0.co;2
614 Hoskins BJ, Valdes PJ (1990) On the existence of storm-tracks. J Atmos Sci
615 47:1854-1864.
616 https://doi.org/10.1175/1520-0469(1990)047<1854:Oteost>2.0.Co;2
617 Jin FF (1997) A theory of interdecadal climate variability of the North Pacific
618 ocean-atmosphere system. J Clim 10:1821-1835.
619 https://doi.org/10.1175/1520-0442(1997)010<1821:atoicv>2.0.co;2
620 Jungclaus J et al. (2006) Ocean circulation and tropical variability in the coupled
621 model ECHAM5/MPI-OM. J Clim 19:3952-3972.
622 https://doi.org/10.1175/JCLI3827.1
623 Keenlyside N, Latif M, Botzet M, Jungclaus J, Schulzweida U (2005) A coupled
624 method for initializing El Niño Southern Oscillation forecasts using sea surface

625 temperature. Tellus A: Dynamic Meteorology and Oceanography 57:340-356.
626 https://doi.org/10.1111/j.1600-0870.2005.00107.x
627 Keenlyside N, Latif M, Jungclaus J, Kornblueh L, Roeckner E (2008) Advancing
628 decadal-scale climate prediction in the North Atlantic sector. Nature 453:84-88.
629 https://doi.org/10.1038/nature06921
630 Kelly KA, Dong S-F (2004) The relationship of western boundary current heat
631 transport and storage to midlatitude ocean-atmosphere interaction. In: Wang C-Z,
632 Xie S-P, Carton JA (eds) Earth's climate: The ocean-atmosphere interaction, vol
633 147. Geophysical Monograph. American Geophysical Union, Washington, DC,
634 pp 347–364
635 Kelly KA, Small RJ, Samelson RM, Qiu B, Joyce TM, Kwon Y-O, Cronin MF (2010)
636 Western boundary currents and frontal air-sea interaction: Gulf Stream and
637 Kuroshio Extension. J Clim 23:5644-5667.
638 https://doi.org/10.1175/2010jcli3346.1
639 Kleeman R, McCreary JP, Klinger BA (1999) A mechanism for generating ENSO
640 decadal variability. Geophys Res Lett 26:1743-1746.
641 https://doi.org/10.1029/1999gl900352
642 Kushnir Y, Lau N-C (1992) The general circulation model response to a North Pacific
643 SST anomaly: Dependence on time scale and pattern polarity. J Clim 5:271-283.
644 https://doi.org/10.1175/1520-0442(1992)005<0271:tgcmrt>2.0.co;2
645 Kushnir Y, Robinson WA, Blade I, Hall NMJ, Peng S-L, Sutton R (2002) Atmospheric
646 GCM response to extratropical SST anomalies: Synthesis and evaluation. J Clim

15:2233-2256. https://doi.org/10.1175/1520-0442(2002)015<2233:agrtes>2.0.co;2

Kuwano-Yoshida A, Minobe S (2017) Storm-track response to SST fronts in the northwestern Pacific region in an AGCM. J Clim 30:1081-1102. https://doi.org/10.1175/jcli-d-16-0331.1

Kwon Y-O, Alexander MA, Bond NA, Frankignoul C, Nakamura H, Qiu B, Thompson LA (2010) Role of the Gulf Stream and Kuroshio-Oyashio Systems in large-scale atmosphere-ocean interaction: A review. J Clim 23:3249-3281. https://doi.org/10.1175/2010jcli3343.1

Kwon Y-O, Deser C (2007) North Pacific decadal variability in the Community Climate System Model version 2. J Clim 20:2416-2433. https://doi.org/10.1175/jcli4103.1

Latif M (2006) On North Pacific multidecadal climate variability. J Clim 19:2906-2915. https://doi.org/10.1175/jcli3719.1

Latif M, Barnett TP (1994) Causes of decadal climate variability over the North Pacific and North America. Science 266:634-637. https://doi.org/10.1126/science.266.5185.634

Latif M, Barnett TP (1996) Decadal climate variability over the North Pacific and North America: Dynamics and predictability. J Clim 9:2407-2423. https://doi.org/10.1175/1520-0442(1996)009<2407:dcvotn>2.0.co;2

Latif M, Keenlyside N (2011) A perspective on decadal climate variability and predictability. Deep Sea Res, Part II 58:1880-1894.

669 https://doi.org/10.1016/j.dsr2.2010.10.066
670 Lau N-C, Holopainen EO (1984) Transient eddy forcing of the time-mean flow as
671 identified by geopotential tendencies. J Atmos Sci 41:313-328.
672 https://doi.org/10.1175/1520-0469(1984)041<0313:Tefott>2.0.Co;2
673 Lee DE, Liu Z-Y, Liu Y (2008) Beyond thermal interaction between ocean and
674 atmosphere: On the extratropical climate variability due to the wind-induced SST.
675 J Clim 21:2001-2018. https://doi.org/10.1175/2007jcli1532.1
676 Lin R-P, Zheng F, Dong X (2018) ENSO frequency asymmetry and the Pacific
677 Decadal Oscillation in observations and 19 CMIP5 models. Adv Atmos Sci
678 35:495-506. https://doi.org/10.1007/s00376-017-7133-z
679 Liu Z-Y, Alexander M (2007) Atmospheric bridge, oceanic tunnel, and global climatic
680 teleconnections. Rev Geophys 45:RG2005.
681 https://doi.org/10.1029/2005RG000172
682 Luo H, Zheng F, Zhu J (2017) Evaluation of oceanic surface observation for
683 reproducing the upper ocean structure in ECHAM5/MPI-OM. J Geophys Res
684 Oceans 122:9695-9711. https://doi.org/10.1002/2017JC013413
685 Ma X-H et al. (2015) Distant influence of Kuroshio eddies on North Pacific weather
686 patterns? Sci Rep 5:17785. https://doi.org/10.1038/srep17785
687 Ma X-H et al. (2016) Western boundary currents regulated by interaction between
688 ocean eddies and the atmosphere. Nature 535:533.
689 https://doi.org/10.1038/nature18640
690 Mantua NJ, Hare SR, Zhang Y, Wallace JM, Francis RC (1997) A Pacific interdecadal

climate oscillation with impacts on salmon production. Bull Am Meteorol Soc 78:1069-1079. https://doi.org/10.1175/1520-0477(1997)078<1069:apicow>2.0.co;2

Marsland SJ, Haak H, Jungclaus J, Latif M, Roske F (2003) The Max-Planck-Institute global ocean/sea ice model with orthogonal curvilinear coordinates. Ocean Model 5:91-127. https://doi.org/10.1016/S1463-5003(02)00015-X

Matsuno T (1966) Quasi-geostrophic motions in the equatorial area. J Meteorol Soc Jpn 44:25-43. https://doi.org/10.2151/jmsj1965.44.1_25

McPhaden MJ, Zhang D-X (2002) Slowdown of the meridional overturning circulation in the upper Pacific Ocean. Nature 415:603-608. https://doi.org/10.1038/415603a

Meehl GA et al. (2014) Decadal prediction: An update from the trenches. Bull Am Meteorol Soc 95:243-267. https://doi.org/10.1175/bams-d-12-00241.1

Nakamura H, Sampe T, Goto A, Ohfuchi W, Xie S-P (2008) On the importance of midlatitude oceanic frontal zones for the mean state and dominant variability in the tropospheric circulation. Geophys Res Lett 35:L15709. https://doi.org/10.1029/2008gl034010

Nakamura H, Sampe T, Tanimoto Y, Shimpo A (2004) Observed associations among storm tracks, jet streams and midlatitude oceanic fronts. In: Wang C-Z, Xie S-P, Carton JA (eds) Earth's climate: The ocean-atmosphere interaction. Geophysical Monograph, vol 147. American Geophysical Union, Washington, DC, pp 329–345

713 Newman M (2007) Interannual to decadal predictability of tropical and North Pacific
714 sea surface temperatures. J Clim 20:2333-2356.
715 https://doi.org/10.1175/jcli4165.1
716 Newman M et al. (2016) The Pacific Decadal Oscillation, revisited. J Clim
717 29:4399-4427. https://doi.org/10.1175/jcli-d-15-0508.1
718 Newman M, Compo GP, Alexander MA (2003) ENSO-forced variability of the
719 Pacific Decadal Oscillation. J Clim 16:3853-3857.
720 https://doi.org/10.1175/1520-0442(2003)016<3853:evotpd>2.0.co;2
721 O'Reilly CH, Czaja A (2015) The response of the Pacific storm track and atmospheric
722 circulation to Kuroshio Extension variability. Q J R Meteorol Soc 141:52-66.
723 https://doi.org/10.1002/qj.2334
724 Papritz L, Spengler T (2015) Analysis of the slope of isentropic surfaces and its
725 tendencies over the North Atlantic. Q J R Meteorol Soc 141:3226-3238.
726 https://doi.org/10.1002/qj.2605
727 Park W, Latif M (2010) Pacific and Atlantic multidecadal variability in the Kiel
728 climate model. Geophys Res Lett 37:L24702.
729 https://doi.org/10.1029/2010gl045560
730 Pierce DW (2001) Distinguishing coupled ocean-atmosphere interactions from
731 background noise in the North Pacific. Prog Oceanogr 49:331-352.
732 https://doi.org/10.1016/s0079-6611(01)00029-5
733 Plaut G, Vautard R (1994) Spells of low-frequency oscillations and weather regimes
734 in the Northern Hemisphere. J Atmos Sci 51:210-236.

735 https://doi.org/10.1175/1520-0469(1994)051<0210:Solfoa>2.0.Co;2
736 Qiu B, Chen S-M (2005) Variability of the Kuroshio Extension jet, recirculation gyre,
737 and mesoscale eddies on decadal time scales. J Phys Oceanogr 35:2090-2103.
738 https://doi.org/10.1175/jpo2807.1
739 Qiu B, Schneider N, Chen S-M (2007) Coupled decadal variability in the North
740 Pacific: An observationally constrained idealized model. J Clim 20:3602-3620.
741 https://doi.org/10.1175/jcli4190.1
742 Roeckner E et al. (2003) The atmospheric general circulation model ECHAM5 - Part I:
743 Model description. Max Planck Institute for Meteorology, Hamburg, Germany
744 Scaife AA, Smith D (2018) A signal-to-noise paradox in climate science. npj Climate
745 and Atmospheric Science 1:28. https://doi.org/10.1038/s41612-018-0038-4
746 Shakun JD, Shaman J (2009) Tropical origins of North and South Pacific decadal
747 variability. Geophys Res Lett 36:L19711. https://doi.org/10.1029/2009gl040313
748 Small RJ et al. (2008) Air–sea interaction over ocean fronts and eddies. Dynamics of
749 Atmospheres and Oceans 45:274-319.
750 https://doi.org/https://doi.org/10.1016/j.dynatmoce.2008.01.001
751 Smith TM, Reynolds RW, Peterson TC, Lawrimore J (2008) Improvements to
752 NOAA's historical merged land-ocean surface temperature analysis (1880-2006).
753 J Clim 21:2283-2296. https://doi.org/10.1175/2007jcli2100.1
754 Solomon A, McCreary JP, Kleeman R, Klinger BA (2003) Interannual and decadal
755 variability in an intermediate coupled model of the Pacific region. J Clim
756 16:383-405. https://doi.org/10.1175/1520-0442(2003)016<0383:Iadvia>2.0.Co;2

757 Sura P, Newman M, Alexander MA (2006) Daily to decadal sea surface temperature
758 variability driven by state-dependent stochastic heat fluxes. J Phys Oceanogr
759 36:1940-1958. https://doi.org/10.1175/jpo2948.1
760 Taguchi B, Nakamura H, Nonaka M, Komori N, Kuwano-Yoshida A, Takaya K, Goto
761 A (2012) Seasonal evolutions of atmospheric response to decadal SST anomalies
762 in the North Pacific subarctic frontal zone: Observations and a coupled model
763 simulation. J Clim 25:111-139. https://doi.org/10.1175/jcli-d-11-00046.1
764 Talley LD, Pickard GL, Emery WJ, Swift JH (2011) Descriptive physical
765 oceanography: An introduction. 6th edn. Academic Press, Boston, MA
766 Trenberth KE (1990) Recent observed interdecadal climate changes in the Northern
767 Hemisphere. Bull Am Meteorol Soc 71:988-993.
768 https://doi.org/10.1175/1520-0477(1990)071<0988:roicci>2.0.co;2
769 Trenberth KE, Branstator G, Karoly DJ, Kumar A, Lau N-C, Ropelewski C (1998)
770 Progress during TOGA in understanding and modeling global teleconnections
771 associated with tropical sea surface temperatures. J Geophys Res Oceans
772 103:14291-14324. https://doi.org/10.1029/97jc01444
773 Trenberth KE, Fasullo JT (2013) An apparent hiatus in global warming? Earth's
774 Future 1:19-32. https://doi.org/10.1002/2013ef000165
775 Valcke S, Caubel A, Declat D, Terray L (2003) OASIS3 ocean atmosphere sea ice soil
776 user’s guide, CERFACS Tech. Rep. TR/CMGC/03/69 edn., Toulouse, France
777 Vimont DJ, Battisti DS, Hirst AC (2001) Footprinting: A seasonal connection between
778 the tropics and mid-latitudes. Geophys Res Lett 28:3923-3926.

779 https://doi.org/10.1029/2001gl013435
780 Vimont DJ, Wallace JM, Battisti DS (2003) The seasonal footprinting mechanism in
781 the Pacific: Implications for ENSO. J Clim 16:2668-2675.
782 https://doi.org/10.1175/1520-0442(2003)016<2668:tsfmit>2.0.co;2
783 Wang L, Chen W, Huang R-H (2008) Interdecadal modulation of PDO on the impact
784 of ENSO on the East Asian winter monsoon. Geophys Res Lett 35:L20702.
785 https://doi.org/10.1029/2008gl035287
786 Wang X-D, Liu H-L (2015) PDO modulation of ENSO effect on tropical cyclone
787 rapid intensification in the western North Pacific. Clim Dyn 46:15-28.
788 https://doi.org/10.1007/s00382-015-2563-8
789 Yanai M, Tomita T (1998) Seasonal and interannual variability of atmospheric heat
790 sources and moisture sinks as determined from NCEP-NCAR reanalysis. J Clim
791 11:463-482. https://doi.org/10.1175/1520-0442(1998)011<0463:saivoa>2.0.co;2
792 Yang Q, Ma Z-G, Xu B-L (2017) Modulation of monthly precipitation patterns over
793 East China by the Pacific Decadal Oscillation. Clim Change 144:405-417.
794 https://doi.org/10.1007/s10584-016-1662-9
795 Zhang L-P, Delworth TL (2015) Analysis of the characteristics and mechanisms of the
796 Pacific Decadal Oscillation in a suite of coupled models from the Geophysical
797 Fluid Dynamics Laboratory. J Clim 28:7678-7701.
798 https://doi.org/10.1175/jcli-d-14-00647.1
799 Zhang L-P, Delworth TL (2016) Simulated response of the Pacific Decadal Oscillation
800 to climate change. J Clim 29:5999-6018. https://doi.org/10.1175/jcli-d-15-0690.1

801 Zheng F (2014) ENSO variability simulated by a coupled general circulation model:
802 ECHAM5/MPI-OM. Atmos Ocean, Sci Lett 7:471-475.
803 https://doi.org/10.3878/j.issn.1674-2834.14.0014
804 Zheng F, Zhu J (2010) Coupled assimilation for an intermediated coupled ENSO
805 prediction model. Ocean Dyn 60:1061-1073.
806 https://doi.org/10.1007/s10236-010-0307-1
807 Zheng F, Zhu J, Zhang R-H (2007) Impact of altimetry data on ENSO ensemble
808 initializations and predictions. Geophys Res Lett 34:L13611.
809 https://doi.org/10.1029/2007GL030451
810 Zheng F, Zhu J, Zhang R-H, Zhou G-Q (2006) Ensemble hindcasts of SST anomalies
811 in the tropical Pacific using an intermediate coupled model. Geophys Res Lett
812 33:L19604. https://doi.org/10.1029/2006GL026994
813 Zhong Y-F, Liu Z-Y, Jacob R (2008) Origin of pacific multidecadal variability in
814 community climate system model, version 3 (CCSM3): A combined statistical
815 and dynamical assessment. J Clim 21:114-133.
816 https://doi.org/10.1175/2007jcli1730.1
817 Zhou G-D, Latif M, Greatbatch RJ, Park W (2015) Atmospheric response to the North
818 Pacific enabled by daily sea surface temperature variability. Geophys Res Lett
819 42:7732-7739. https://doi.org/10.1002/2015gl065356
820

List of figures

Figure 1. PDO in the observation (left panel) and the simulation (right panel). The leading empirical orthogonal function (EOF) of monthly sea surface temperature in (a) and (b). The associated PC time series, regarded as the PDO index, showing the unsmoothed record (red and blue bars) and the 10-year low-pass-filtered record (black line) in (c) and (d). The power spectral density of low-pass-filtered record (blue line) and associated 95% confidence interval (red dashed line).

Figure 2. Positive minus negative PDO phases composite of SLP (unit: hPa) as well as SST (unit: °C) at sea surface (top two panels); and geopotential height (unit: gpm) as well as air temperature (unit: °C) at 500hPa and 100hPa (lower six panels). The shading is for SST and air temperature, and the contours are for SLP and geopotential height with the solid (dashed) line denoting the positive (negative) value. The green line in the first row represents the negative climatological meridional SST gradient (unit: °C/110km).

Figure 3. The influence of ocean on the atmosphere during peak phase of the PDO between 20°N–60°N, and 150°E–150°W (indicated by the yellow box in Fig. 2). Regression of the PDO index against anomalous (a) negative meridional temperature gradient (orange solid, unit: °C/110km), net heat flux (yellow solid, unit: W/m^2), latent heat flux (purple solid, unit: W/m^2), sensible heat flux (green solid, unit: W/m^2), surface zonal wind (light blue dashed, unit: m/s), SST (brown dashed, unit: °C), evaporation minus precipitation (purple dashed, unit: m/s), and SST minus SAT (green dashed). Latitude–altitude sections of the regression of the PDO index against

anomalies of (b) negative meridional air temperature gradient (unit: °C/110km), and (c) Eady growth rate (unit: /day) at surface zonally averaged over the Western North Pacific (150°E–150°W). Heat flux is defined as positive downwards. The climatology of the negative of the meridional SST gradient is overlaid in (a, dark blue, unit: °C/110km). The dots in (b, c) indicate the regions passing the F-test at 95 % significant level.

Figure 4. Latitude–altitude sections of the regression of the PDO index against anomalies of (a) diabatic heating (i.e., Qd), (b) transient eddy heating (i.e., Qeddy), (c) transient eddy vorticity forcing (i.e., Feddy), and (d) geopotential height zonally averaged over the Western North Pacific (150°E–150°W).

Figure 5. The influence of atmosphere on the ocean during the peak phase of the PDO between 150°E–150°W, and 20°N–60°N. Regression of the PDO index against (a) zonal wind at 1000hPa (shading, unit: m/s), and (b) SST tendencies induced by advections (shading, unit: °C/s). The dots in (a, b) indicate the regions passing the F-test at 95 % significant level. The regressed anomalies of SST upon the PDO index (contour, unit: °C) are also shown in (a, b).

Figure 6. Schematic for local positive feedback of PDO in the mid-latitude North Pacific.

Figure 7. Atmospheric circulation driving the negative oceanic feedback of PDO on decadal time scales. The correlation between the PDO index and the North Pacific wind stress curl field (a), as well as (b) the lagged correlation between the PDO index and the wind stress curl index (green box, 170°E - 150°W and 20°N - 36°N). The dots

865 in (a) indicate the regions passing the F-test at 95 % significant level. The box used to
866 for analysis of the meridional sections is also shown (yellow).

867 **Figure 8.** The impact of atmosphere in driving an ocean mediated negative feedback
868 of PDO on decadal time scales. Lagged correlation between the wind stress curl index
869 and the North Pacific OHC700 field. Lags are for the following: (a)–(d) 0, 6, 12, and
870 18 yr. The yellow (green) box in (a) denotes the region for Kuroshio (KOE) in Fig.
871 9b.

872 **Figure 9.** The role of oceanic Rossby wave in the negative feedback of PDO on
873 decadal time scales. Lagged correlation of SSH along the zonal band of 20°–25°N
874 against the PDO index.

875 **Figure 10.** Lagged correlation between PDO index and each term of the upper 700m
876 ocean temperature equation for (a) Kuroshio and (b) KOE regions. Blue, red, yellow,
877 purple, green, and cyan lines indicate temperature tendency, temperature, zonal
878 advection, meridional advection, vertical advection, and net surface heat flux,
879 respectively. Dashed, dotted, and dash-dotted lines indicate contributions by the
880 anomalous temperature, anomalous current and nonlinear advection terms,
881 respectively. Thick lines indicate the >95% confidence level based on the t-test.

882 **Figure 11.** Composite of SST anomalies (°C, first column), OHC700 (10^{18}J, second
883 column), and wind stress curl anomalies (10^{-8}Pa·s^{-1}·m^{-1}, third column) keyed to phase
884 categories 1-4 (first to fourth row) of the decadal oscillation.

885 **Figure 12.** Schematic for negative feedback of PDO in the mid-latitude North Pacific.

886

Figure 1

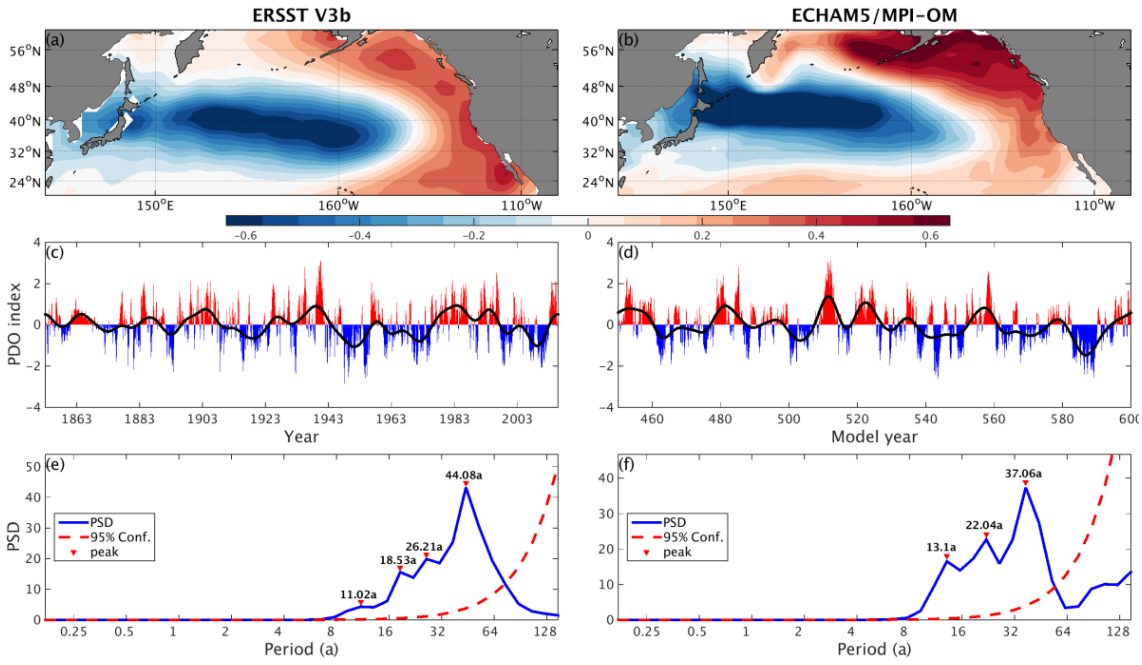

887

888 **Figure 1.** PDO in the observation (left panel) and the simulation (right panel). The

889 leading empirical orthogonal function (EOF) of monthly sea surface temperature in (a)

890 and (b). The associated PC time series, regarded as the PDO index, showing the

891 unsmoothed record (red and blue bars) and the 10-year low-pass-filtered record (black

892 line) in (c) and (d). The power spectral density of low-pass-filtered record (blue line)

893 and associated 95% confidence interval (red dashed line).

894

Figure 2

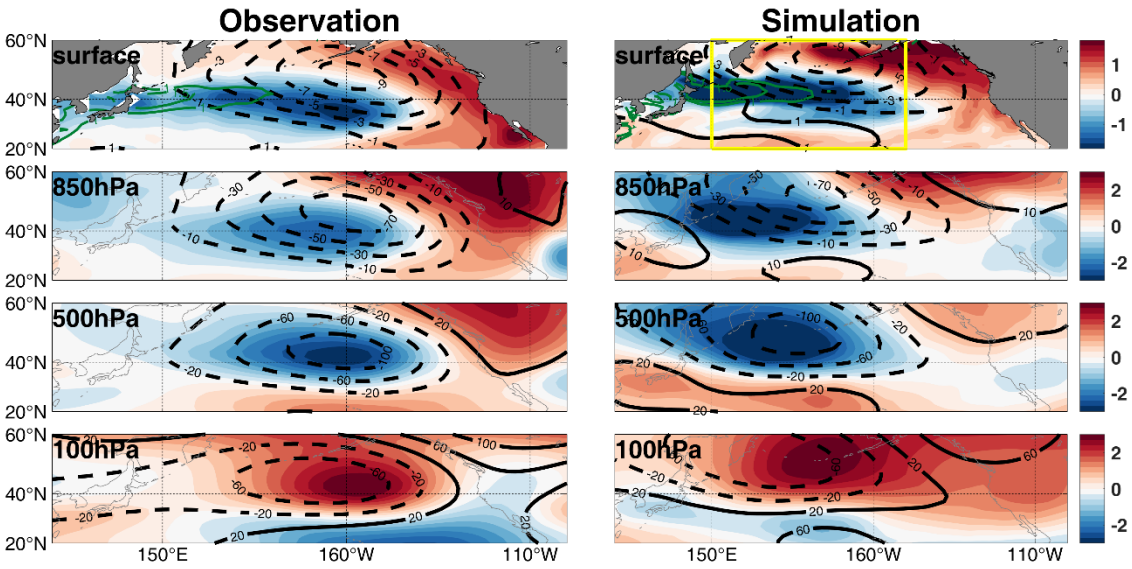

Figure 2. Positive minus negative PDO phases composite of SLP (unit: hPa) as well as SST (unit: °C) at sea surface (top two panels); and geopotential height (unit: gpm) as well as air temperature (unit: °C) at 500hPa and 100hPa (lower six panels). The shading is for SST and air temperature, and the contours are for SLP and geopotential height with the solid (dashed) line denoting the positive (negative) value. The green line in the first row represents the negative climatological meridional SST gradient (unit: °C/110km).

Figure 3

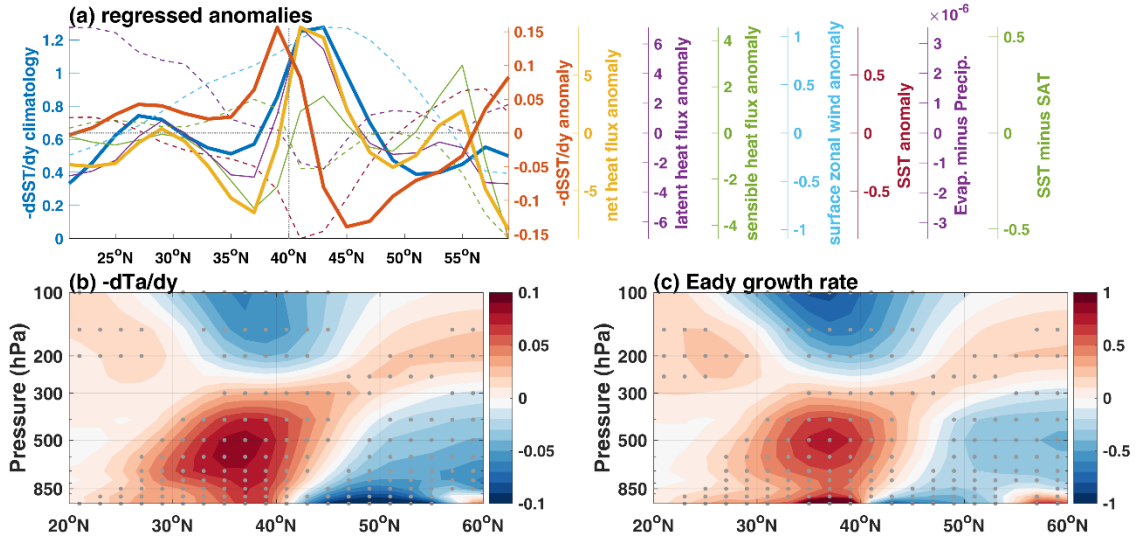

Figure 3. The influence of ocean on the atmosphere during peak phase of the PDO between 20°N–60°N, and 150°E–150°W (indicated by the yellow box in Fig. 2). Regression of the PDO index against anomalous (a) negative meridional temperature gradient (orange solid, unit: °C/110km), net heat flux (yellow solid, unit: W/m^2), latent heat flux (purple solid, unit: W/m^2), sensible heat flux (green solid, unit: W/m^2), surface zonal wind (light blue dashed, unit: m/s), SST (brown dashed, unit: °C), evaporation minus precipitation (purple dashed, unit: m/s), and SST minus SAT (green dashed). Latitude–altitude sections of the regression of the PDO index against anomalies of (b) negative meridional air temperature gradient (unit: °C/110km), and (c) Eady growth rate (unit: /day) at surface zonally averaged over the Western North Pacific (150°E–150°W). Heat flux is defined as positive downwards. The climatology of the negative of the meridional SST gradient is overlaid in (a, dark blue, unit: °C/110km). The dots in (b, c) indicate the regions passing the F-test at 95 % significant level.

922 **Figure 4**

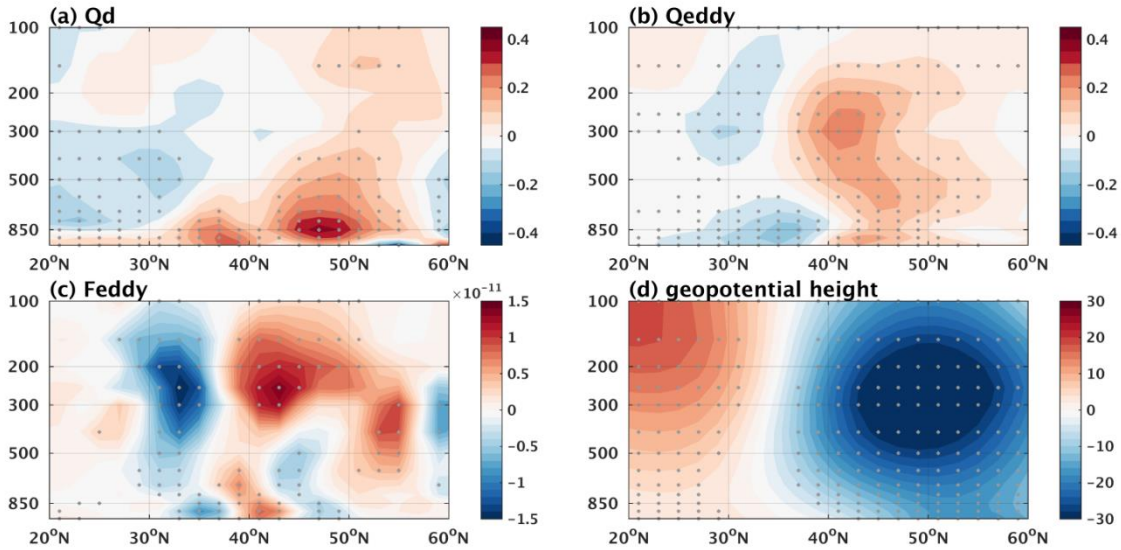

923

924 **Figure 4.** Latitude–altitude sections of the regression of the PDO index against
925 anomalies of (a) diabatic heating (i.e., Qd), (b) transient eddy heating (i.e., Qeddy), (c)
926 transient eddy vorticity forcing (i.e., Feddy), and (d) geopotential height zonally
927 averaged over the Western North Pacific (150°E–150°W).

928

929 **Figure 5**

930 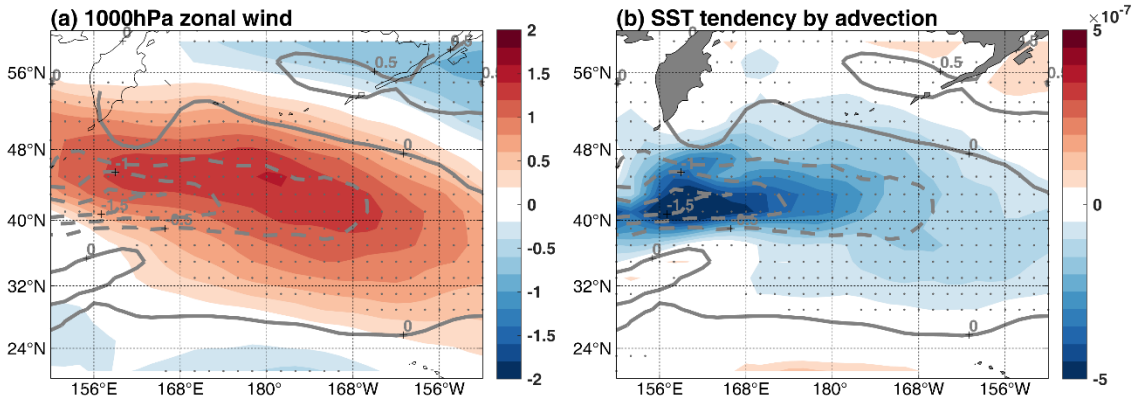

931 **Figure 5.** The influence of atmosphere on the ocean during the peak phase of the

932 PDO between 150°E–150°W, and 20°N–60°N. Regression of the PDO index against

933 (a) zonal wind at 1000hPa (shading, unit: m/s), and (b) SST tendencies induced by

934 advections (shading, unit: °C/s). The dots in (a, b) indicate the regions passing the

935 F-test at 95 % significant level. The regressed anomalies of SST upon the PDO index

936 (contour, unit: °C) are also shown in (a, b).

937

938 **Figure 6**

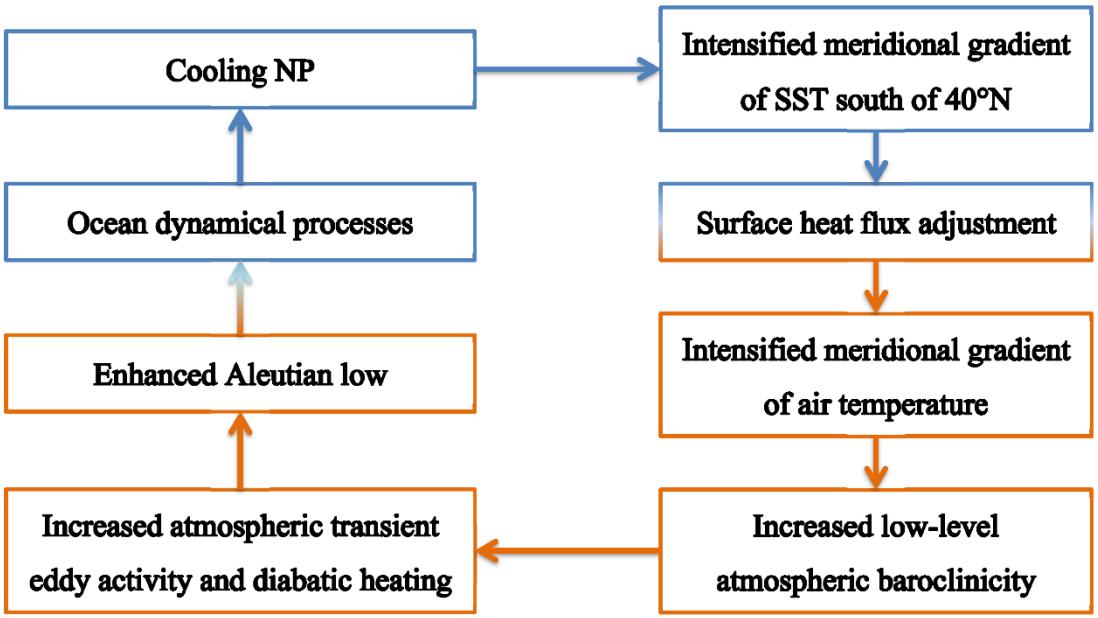

939

940 **Figure 6.** Schematic for local positive feedback of PDO in the mid-latitude North

941 Pacific.

942

943 **Figure 7**

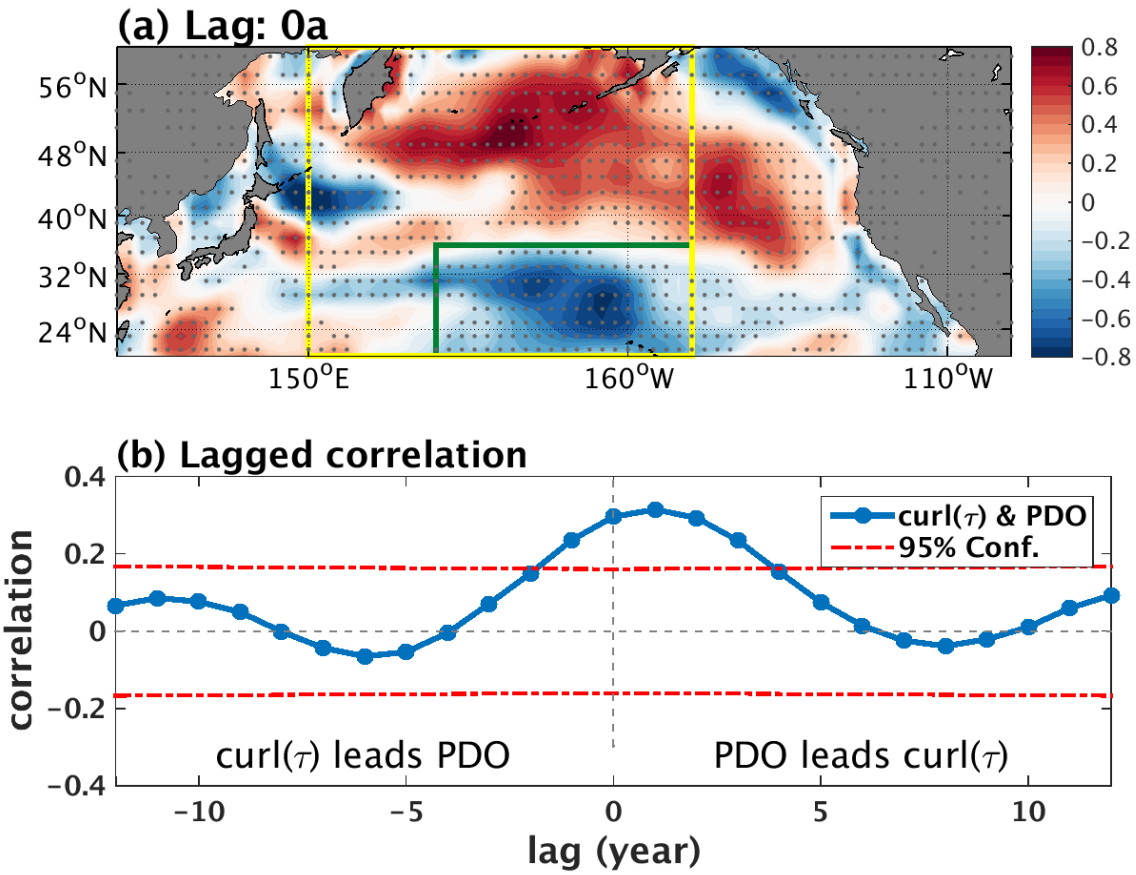

944

945 **Figure 7.** Atmospheric circulation driving the negative oceanic feedback of PDO on
946 decadal time scales. The correlation between the PDO index and the North Pacific
947 wind stress curl field (a), as well as (b) the lagged correlation between the PDO index
948 and the wind stress curl index (green box, 170°E - 150°W and 20°N - 36°N). The dots
949 in (a) indicate the regions passing the F-test at 95 % significant level. The box used to
950 for analysis of the meridional sections is also shown (yellow).

951

952 **Figure 8**

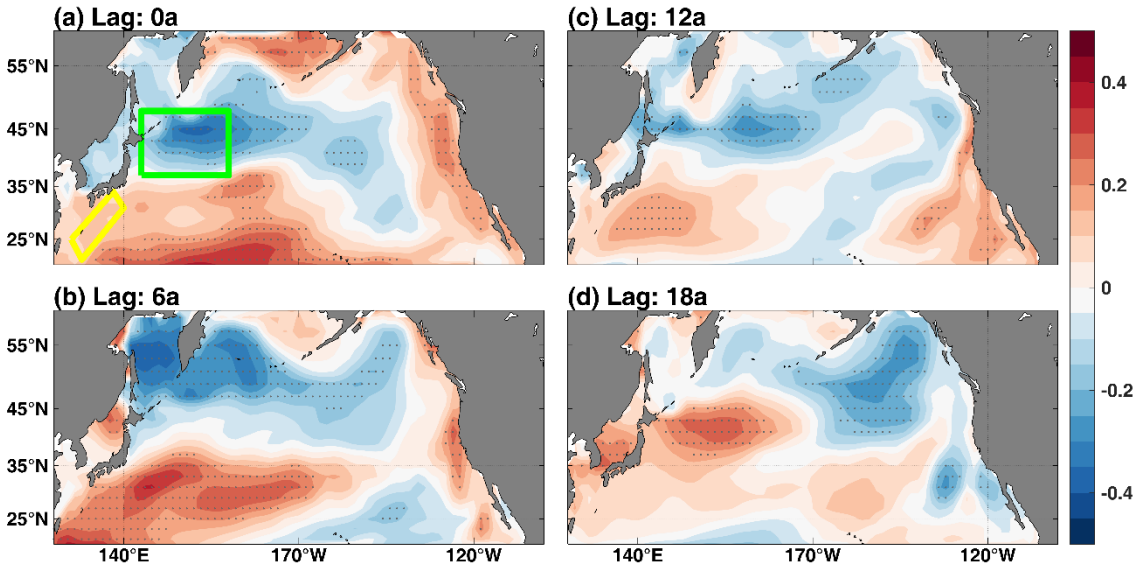

953

954 **Figure 8.** The impact of atmosphere in driving an ocean mediated negative feedback

955 of PDO on decadal time scales. Lagged correlation between the wind stress curl index

956 and the North Pacific OHC700 field. Lags are for the following: (a)–(d) 0, 6, 12, and

957 18 yr. The yellow (green) box in (a) denotes the region for Kuroshio (KOE) in Fig.

958 10.

959

960 **Figure 9**

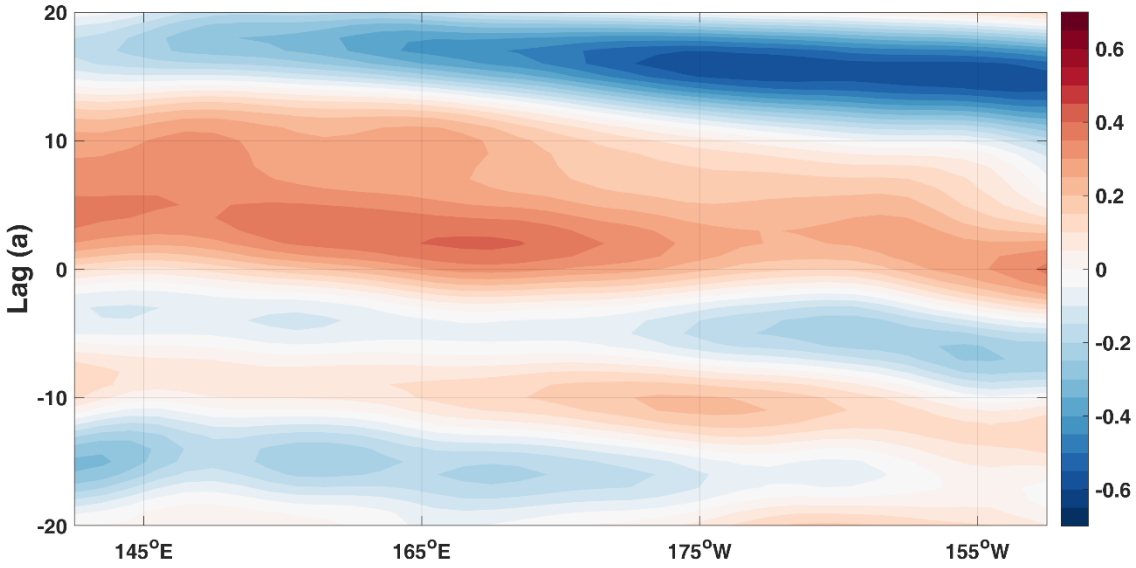

961

962 **Figure 9.** The role of oceanic Rossby wave in the negative feedback of PDO on

963 decadal time scales. Lagged correlation of SSH along the zonal band of 20°–25°N

964 against the PDO index.

965

966 **Figure 10**

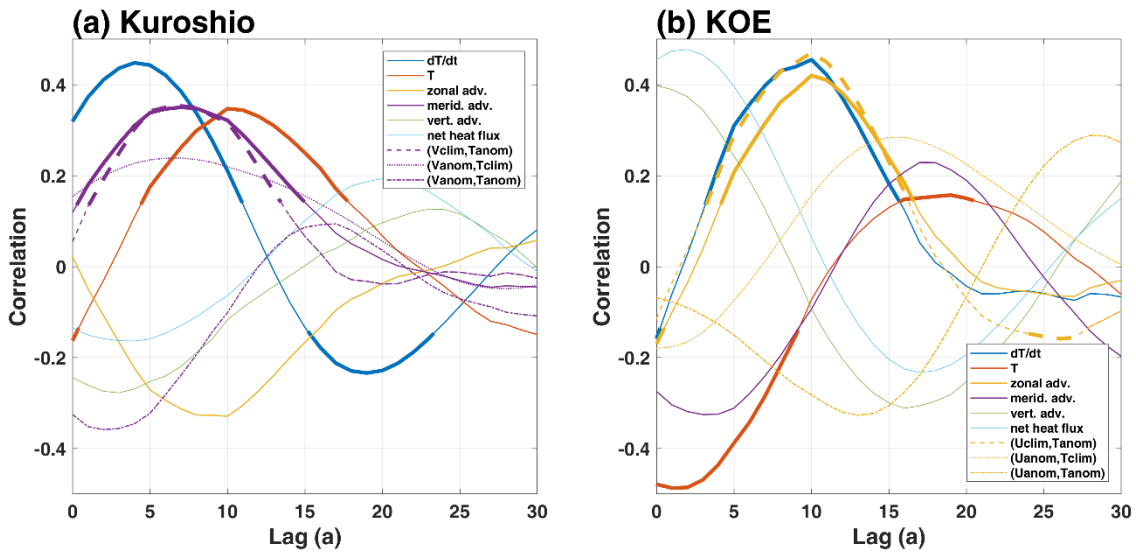

967

968 **Figure 10.** Lagged correlation between PDO index and each term of the upper 700m
969 ocean temperature equation for (a) Kuroshio and (b) KOE regions. Blue, red, yellow,
970 purple, green, and cyan lines indicate temperature tendency, temperature, zonal
971 advection, meridional advection, vertical advection, and net surface heat flux,
972 respectively. Dashed, dotted, and dash-dotted lines indicate contributions by the
973 anomalous temperature, anomalous current and nonlinear advection terms,
974 respectively. Thick lines indicate the >95% confidence level based on the t-test.

975

976 **Figure 11**

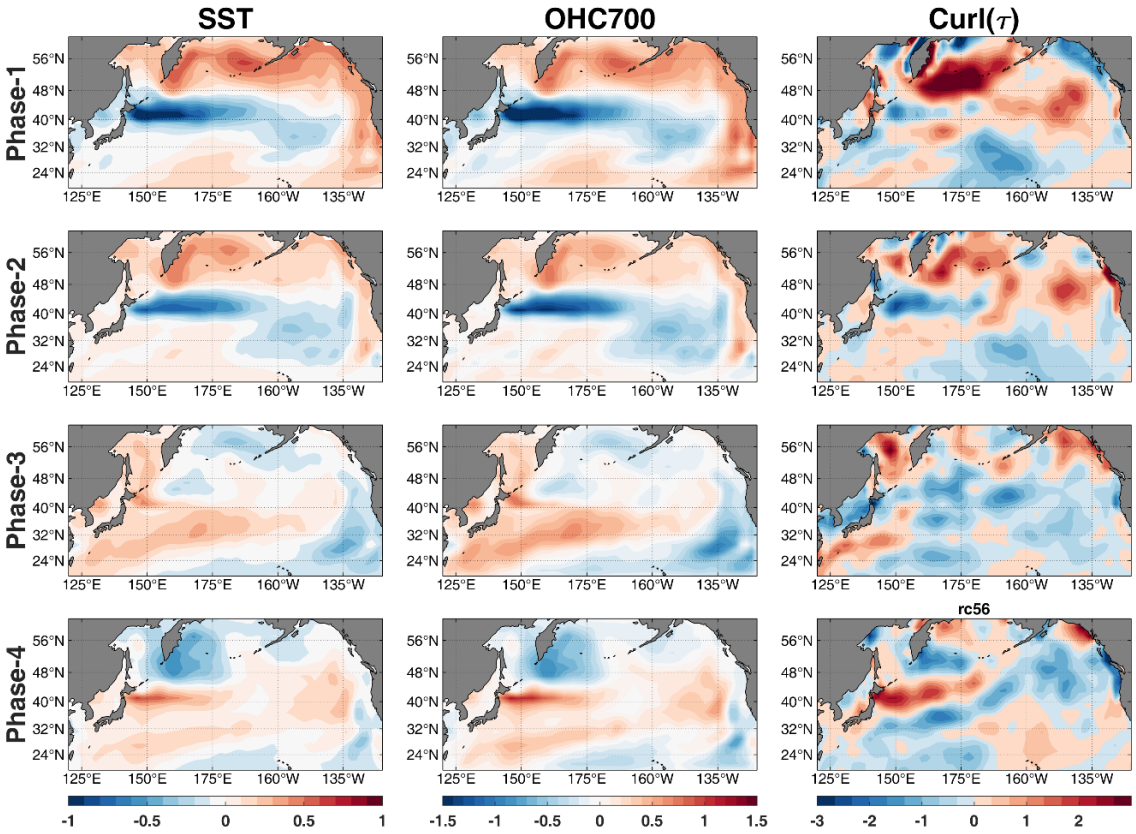

977

978 **Figure 11.** Composite of SST anomalies (°C, first column), OHC700 (10^{18}J, second

979 column), and wind stress curl anomalies (10^{-8}Pa·s^{-1}·m^{-1}, third column) keyed to phase

980 categories 1-4 (first to fourth row) of the decadal oscillation.

981

982 **Figure 12**

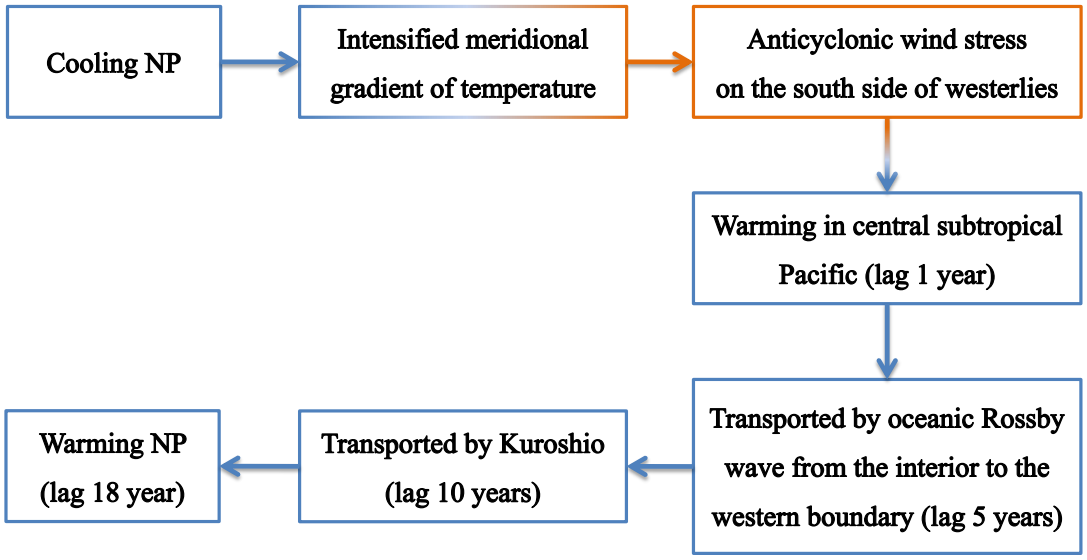

983

984 **Figure 12.** Schematic for negative feedback of PDO in the mid-latitude North Pacific.

985